



# N-acyl-O-phosphocholineserines: structures of a novel class of lipids that are biomarkers for Niemann-Pick C1 disease

Rohini Sidhu,\* Yawo Mondjinou,\* Mingxing Qian,<sup>†</sup> Haowei Song,<sup>§</sup> Arun Babu Kumar,\*\* Xinying Hong,\*\* Fong-Fu Hsu,\* Dennis J. Dietzen,<sup>††</sup> Nicole M. Yanjanin,<sup>§§</sup> Forbes D. Porter,<sup>§§</sup> Elizabeth Berry-Kravis,\*\*\* Charles H. Vite,<sup>†††</sup> Michael H. Gelb,\*\* Jean E. Schaffer,\* Daniel S. Ory,\* and Xuntian Jiang<sup>1,\*</sup>

Departments of Medicine,\* Developmental Biology,<sup>†</sup> and Pediatrics,<sup>††</sup> Washington University School of Medicine, St. Louis, MO 63110; Process and Analytical Development,<sup>§</sup> MilliporeSigma, St. Louis, MO 63118; Department of Chemistry,\*\* University of Washington, Seattle, WA 98195; Section on Molecular Dysmorphology,<sup>§§</sup> Eunice Kennedy Shriver National Institute of Child Health and Human Development, National Institutes of Health, Department of Health and Human Services, Bethesda, MD 20892; Departments of Pediatrics, Neurological Sciences, and Biochemistry,\*\*\* Rush University Medical Center, Chicago, IL 60612; and Department of Clinical Studies and Advanced Medicine,<sup>†††</sup> University of Pennsylvania School of Veterinary Medicine, Philadelphia, PA 70736

ORCID IDs: 0000-0002-4954-6659 (J.E.S.); 0000-001-9048-7294 (X.J.)

**Abstract** Niemann-Pick disease type C1 (NPC1) is a fatal, neurodegenerative, cholesterol storage disorder. With new therapeutics in clinical trials, there is an urgency to improve diagnostics and monitor therapeutic efficacy with biomarkers. In this study, we sought to define the structure of an unknown lipid biomarker for NPC1 with  $[M + H]^+$  ion at  $m/z$  509.3351, previously designated as lysoSM-509. The structure of N-palmitoyl-O-phosphocholineserine (PPCS) was proposed for the lipid biomarker based on the results from mass spectrometric analyses and chemical derivatizations. As no commercial standard is available, authentic PPCS was chemically synthesized, and the structure was confirmed by comparison of endogenous and synthetic compounds as well as their derivatives using liquid chromatography-tandem mass spectrometry (LC-MS/MS). PPCS is the most abundant species among N-acyl-O-phosphocholineserines (APCS), a class of lipids that have not been previously detected in biological samples. Further analysis demonstrated

that all APCS species with acyl groups ranging from C14 to C24 were elevated in NPC1 plasma. PPCS is also elevated in both central and peripheral tissues of the NPC1 cat model. Identification of APCS structures provide an opportunity for broader exploration of the roles of these novel lipids in NPC1 disease pathology and diagnosis.—Sidhu, R., Y. Mondjinou, M. Qian, H. Song, A. B. Kumar, X. Hong, F.F. Hsu, D. J. Dietzen, N. M. Yanjanin, F. D. Porter, E. Berry-Kravis, C. H. Vite, M. H. Gelb, J. E. Schaffer, D. S. Ory, and X. Jiang. N-acyl-O-phosphocholineserines: structures of a novel class of lipids that are biomarkers for Niemann-Pick C1 disease. *J. Lipid Res.* 2019. 60: 1410–1424.

**Supplementary key words** Niemann-Pick disease type C • mass spectrometry • structural identification • lysoSM-509

Niemann-Pick disease type C (NPC) is a rare neurovisceral disorder caused by mutations of *NPC1* (95% of NPC cases) (1) or *NPC2* (2) and characterized by accumulation of unesterified cholesterol and glycosphingolipids in late endosomes/lysosomes (3). The impaired lipid trafficking is associated with neuron loss and defective myelination, leading to neuroinflammatory and neurodegenerative disease pathology (4). NPC1 disease shows substantial

Abbreviations: APCS, N-acyl-O-phosphocholineserine; d<sub>5</sub>-PPCS, (S)-N-d<sub>5</sub>-palmitoyl-O-phosphocholineserine; HCD, higher energy collisional dissociation; H/D, hydrogen/deuterium; MRM, multiple reaction monitoring; NPC, Niemann-Pick disease type C; PPCS, N-palmitoyl-O-phosphocholineserine.

<sup>1</sup>To whom correspondence should be addressed.  
e-mail: jiangxuntian@wustl.edu

Copyright © 2019 Sidhu et al. Published under exclusive license by The American Society for Biochemistry and Molecular Biology, Inc.  
This article is available online at <http://www.jlr.org>

This work was supported by National Institutes of Health Clinical and Translational Science Award UL1 TR000448 (X.J.) and Grants R01 NS081985 (D.S.O. and J.E.S.), P41-GM103422 (F.F.H.), and 2R01DK067859 (M.H.G.); grants from the University of Pennsylvania Orphan Disease Center (X.J.), Dana's Angels Research Trust (D.S.O. and N.M.Y.), and Ara Parseghian Medical Research Foundation (D.S.O. and N.M.Y.); support from Accelerated Research for NPC Disease (D.S.O.), Hope for Hayley and Samantha's Search for the Cure Funds (E.B.K.), and Referral Center for Animal Models of Human Genetic Disease (National Institutes of Health Grant P40 OD010939; C.H.V.). This study was also supported by the intramural research program of the Eunice Kennedy Shriver National Institute of Child Health and Human Development (F.D.P.) and a Bench to Bedside Award from the Office of Rare Diseases (F.D.P. and D.S.O.). This work was performed in the Metabolomics Facility at Washington University (National Institutes of Health Grant P30 DK020579). The content is solely the responsibility of the authors and does not necessarily represent the official views of the National Institutes of Health.

Manuscript received 24 May 2019 and in revised form 13 June 2019.

Published, JLR Papers in Press, June 14, 2019

DOI <https://doi.org/10.1194/jlr.RA119000157>

heterogeneity in age of onset and systemic, neurological, and psychiatric signs and symptoms (5). The heterogeneity of disease presentation and lack of specific symptoms complicate diagnosis, leading to an average diagnostic delay of 4–5 years (6). As currently available treatments, such as miglustat (7) and 2-hydroxypropyl- $\beta$ -cyclodextrin (8–10), can only stabilize or slow disease progression, early initiation of treatment prior to onset of neurologically symptomatic disease is essential.

In recent years, diagnosis of NPC1 disease has been greatly facilitated by discovery of sensitive and specific biomarkers that are elevated in blood from NPC patients. The most promising of these include oxysterols (11–23), lysosphingomyelin (24), *N*-(3 $\beta$ ,5 $\alpha$ ,6 $\beta$ -trihydroxy-cholan-24-oyl) glycine (designated as bile acid B) (25, 26), and an unknown lipid (lysoSM-509) (27–31). The oxysterol, cholestane-3 $\beta$ ,5 $\alpha$ ,6 $\beta$ -triol, is the most widely disseminated biomarker and has been implemented on multiple platforms in ~50 laboratories worldwide. In combination with genetic analyses, oxysterols have become a first line diagnostic test (32). lysoSM-509 showed similar diagnostic potential to cholestane-3 $\beta$ ,5 $\alpha$ ,6 $\beta$ -triol (27), though application of this biomarker has been limited because its structure is unknown. Herein, we performed structural analysis of lysoSM-509 to show that it is *N*-palmitoyl-*O*-phosphocholineserine (PPCS), the most abundant species of a class of lipids, *N*-acyl-*O*-phosphocholineserines (APCSs). To the best of our knowledge, this is the first description of this lipid class.

## MATERIALS AND METHODS

### Human subjects

Human studies adhered to the principles of the Declaration of Helsinki, as well as to Title 45, US Code of Federal Regulations, Part 46, Protection of Human Subjects. Informed consent was obtained from the human subjects or their representatives. NPC1 plasma and dried blood spot samples were obtained from the National Institutes of Health and Rush University Medical Center. All NPC1 and NPC1 carrier dried blood spots were de-identified and collected from previously diagnosed patients and obligate heterozygotes, respectively. Normal plasma and dried blood spots were obtained from anonymized residual samples at St. Louis Children's Hospital. Whole blood, plasma, red blood cells, and white blood cells were collected from four healthy adult volunteers. Collection and analysis of de-identified human samples were approved by the institutional review boards at Washington University, Eunice Kennedy Shriver National Institute of Child Health and Human Development, and Rush University Medical Center.

### Experimental animals

BALB/c *Npc<sup>nih</sup>* (*Npc1<sup>-/-</sup>*) mice were obtained from Jackson Laboratories (Bar Harbor, ME) and were maintained in a breeding colony at Washington University. NPC1 cats were raised in the animal colony of the School of Veterinary Medicine at the University of Pennsylvania under National Institutes of Health and US Department of Agriculture guidelines for the care and use of animals in research. Serum/plasma, liver, and brain samples were collected from 24- to 25-week-old cats and 7-week-old mice. Experimental procedures were approved by the Washington

University and University of Pennsylvania Animal Studies Committees and were conducted in accordance with the US Department of Agriculture Animal Welfare Act and the Public Health Service Policy for the Humane Care and Use of Laboratory Animals.

### Profiling of lysoSM-509 in human plasma and dried blood spots

lysoSM-509 was extracted from plasma samples (50  $\mu$ l) and dried blood spot discs (3 mm) and submitted to LC-MS/MS. The detailed protocols are described in the supplemental information.

### lysoSM-509 structure identification

*LC-HRMS of endogenous lysoSM-509 and synthetic PPCS.* The lysoSM-509 isolated from plasma was reconstituted in methanol and submitted to the LC-high-resolution MS (LC-HRMS) assay described in the supplemental information.

*Hydrogen/deuterium exchange experiment.* The hydrogen/deuterium (H/D) exchange experiment of isolated lysoSM-509 was conducted on a Shimadzu Prominence HPLC system coupled with the Applied Biosystems/MDS Sciex 4000QTRAP mass spectrometer operating in positive multiple reaction monitoring (MRM) mode, as described in the supplemental information.

*Derivatization.* Derivatization of lysoSM-509, including methyl esterification, acylation, ozonolysis, and alkaline degradation, and LC-MS/MS analysis of derivatized lysoSM-509 and synthetic PPCS are described in the supplemental information.

### Synthesis of PPCS, d<sub>5</sub>-PPCS, and potential precursors for PPCS bioanalysis

*N-palmitoyl-L-serine methyl ester (2a).* To a solution of *N*-succinimidyl palmitate (1.35 g, 3.82 mmol, 1 eq) in dichloromethane (15 ml) was added L-serine methyl ester hydrochloride (**1a**) (1.23 g, 7.93 mmol, 2.1 eq) and triethylamine (1.21 ml, 8.73 mmol, 2.28 eq), and the mixture was stirred at room temperature overnight. The solution was loaded on a silica column and purified with chromatography (dichloromethane/methanol, 10/1) to give **2a** (1.19 g, 87%), mp: 86–87°C. <sup>1</sup>H NMR (400 MHz, CDCl<sub>3</sub>)  $\delta$  6.58 (d, *J* = 6.7 Hz, 1H), 4.51 (dt, *J* = 3.6, 6.7 Hz, 1H), 3.92 (dd, *J* = 3.6, 11.1, 1H), 3.86 (d, *J* = 11.1, 1H), 3.73 (s, 3H), 2.22 (t, *J* = 6.9 Hz, 2H), 1.64–1.54 (m, 2H), 1.27–1.18 (m, 24H), 0.83 (t, *J* = 6.9, 3H). <sup>13</sup>C NMR (100 MHz, CDCl<sub>3</sub>)  $\delta$  173.98, 171.65, 63.23, 54.59, 52.68, 36.48, 31.82, 29.70, 29.67, 29.66, 29.64, 29.52, 29.37, 29.36, 29.26, 25.59, 22.69, 14.12.

*(S)-N-palmitoyl-O-H-phosphonate-serine methyl ester (3a).* A solution of imidazole (2.38 g, 35 mmol, 25 eq) in dichloromethane (25 ml) was cooled to –10°C, followed by addition of phosphorus trichloride (0.611 ml, 7 mmol, 5 eq) and triethylamine (2.92 ml, 21 mmol, 15 eq). The reaction mixture was stirred for 30 min at –10°C. A solution of compound **2a** (500 mg, 1.4 mmol, 1 eq) in dichloromethane (20 ml) was added dropwise to the reaction mixture using a syringe pump over a period of 90 min. After the addition, the mixture was stirred for 40 min further and quenched by addition of water (10 ml). The resulting solution was stirred for an additional period of 5 min. The organic layer was washed with brine (10 ml). The aqueous phase was extracted with tetrahydrofuran until it became a clear solution. The combined organic phases were dried with sodium sulfate and concentrated. The residue was dried over phosphorus pentoxide under high vacuum overnight to give 0.91 g of crude **3a**.

(*S*)-*N*-palmitoyl-*O*-phosphocholineserine methyl ester (**5a**). A mixture of crude **3a** (1.4 mmol, 1 eq) and choline tetraphenylborate (1.18 g, 2.8 mmol, 2 eq) was dried by evaporation with anhydrous pyridine (10 ml). The mixture was dissolved in pyridine (10 ml), and 2-chloro-5,5-dimethyl-1,3,2-dioxaphosphorinane 2-oxide (0.775 g, 4.2 mmol, 3 eq) was added. The resulting mixture was stirred for 15 min to give **4a**. Iodine (0.427 g, 1.68 mmol, 1.2 eq) dissolved in pyridine (3 ml) and water (0.2 ml) was added and the mixture was stirred for 10 min. The solution was washed with 5% (w/v) aqueous solution of sodium bisulfite until the color faded. The mixture was concentrated to give crude **5a**, which was confirmed as PPCS methyl ester by LC-MS/MS. The **5a** was completely degraded to decomposition products 1 and 2 by alkaline hydrolysis at room temperature for 60 h.

*N*-palmitoyl-*L*-serine *tert*-butyl ester (**2b**). The **2b** was prepared as a white solid from *N*-succinimidyl palmitate (1.3 g, 3.68 mmol, 1 eq), *L*-serine *tert*-butyl ester hydrochloride (**1b**) (1.53 g, 7.73 mmol, 2.1 eq), and triethylamine (1.17 ml, 8.4 mmol, 2.28 eq) according to the procedure described for the preparation of **2a** (1.45 g, 99%), mp: 64–65°C. <sup>1</sup>H NMR (400 MHz, CDCl<sub>3</sub>) δ 6.58 (d, *J* = 6.7 Hz, 1H), 4.51 (dt, *J* = 3.5, 6.7 Hz, 1H), 3.85 (d, *J* = 3.5 Hz, 2H), 2.22 (t, *J* = 6.9 Hz, 2H), 1.66–1.55 (m, 2H), 1.45 (s, 9H), 1.27–1.18 (m, 24H), 0.83 (t, *J* = 6.9, 3H). <sup>13</sup>C NMR (100 MHz, CDCl<sub>3</sub>) δ 173.82, 169.59, 82.54, 63.71, 55.30, 55.27, 36.47, 31.84, 29.61, 29.58, 29.54, 29.41, 29.28, 29.21, 27.90, 25.53, 22.60, 14.02.

(*S*)-*N*-palmitoyl-*O*-*H*-phosphonate-serine *tert*-butyl ester (**3b**). The **3b** was prepared from **2b** (0.94 g, 2.35 mmol, 1 eq), imidazole (4 g, 58.75 mmol, 25 eq), phosphorus trichloride (1.03 ml, 11.75 mmol, 5 eq), and triethylamine (4.9 ml, 35.25 mmol, 15 eq) according to the procedure described for the preparation of **3a**. The crude **3b** was used directly in the next step without purification.

(*S*)-*N*-palmitoyl-*O*-phosphocholineserine *tert*-butyl ester (**5b**). The **5b** was prepared from crude **3b** (prepared as above), choline tetraphenylborate (1.99 g, 4.7 mmol, 2 eq), 2-chloro-5,5-dimethyl-1,3,2-dioxaphosphorinane 2-oxide (1.3 g, 7.05 mmol, 3 eq), iodine (0.716 g, 2.82, 1.2 eq), and water (0.4 ml) according to the procedure described for the preparation of **5a**. The crude **5b** was used directly in the next step without purification.

(*S*)-*N*-palmitoyl-*O*-phosphocholineserine. A suspension of crude **5b** (prepared as above) in trifluoroacetic acid (27 ml) and chloroform (27 ml) was stirred at room temperature for 1 day and evaporated to dryness. The residue was chromatographed on C18 silica (methanol-water, 7/3). The PPCS was further purified with chromatography on silica with chloroform-methanol-water (50:49:1) to give a white solid (225 mg, 19% overall yield from **2b**), mp: 220–221°C. <sup>1</sup>H NMR (400 MHz, CD<sub>3</sub>OD) δ 4.87 (s, 1H), 4.36 (d, 1H, *J* = 1.1 Hz), 4.22 (m, 2H), 4.07 (m, 1H), 3.58 (dd, 2H, *J* = 4.3, 6.2 Hz), 3.26 (d, 1H, *J* = 1.1 Hz), 3.17 (s, 9H), 2.22 (t, 2H, *J* = 7.6 Hz), 1.57 (m, 2H), 1.23 (m, 24H), 0.85 (t, 2H, *J* = 7.6 Hz). <sup>13</sup>C NMR (100 MHz, CD<sub>3</sub>OD) δ 176.03, 175.64, 68.08, 68.03, 60.58, 60.53, 56.73, 56.63, 54.87, 54.84, 54.80, 37.47, 33.24, 30.97, 30.93, 30.83, 30.72, 30.67, 30.65, 27.03, 23.90, 14.62.

*N*-*d*<sub>5</sub>-palmitoyl-*L*-serine *tert*-butyl ester (**2c**). The **2c** was prepared as a white solid from *N*-succinimidyl-*d*<sub>5</sub>-palmitate (0.67 g, 1.87 mmol, 1 eq), *L*-serine *tert*-butyl ester hydrochloride (**1b**) (0.776 g, 3.93 mmol, 2.1 eq), and triethylamine (0.593 ml, 4.26 mmol, 2.28 eq) according to the procedure described for the preparation of **2a** (0.71 g, 93%), mp: 64–65°C. <sup>1</sup>H NMR (400 MHz,

CDCl<sub>3</sub>) δ 6.53 (d, *J* = 6.7 Hz, 1H), 4.53 (dt, *J* = 3.5, 6.7 Hz, 1H), 3.88 (d, *J* = 3.5 Hz, 2H), 3.22 (s, br, 1H), 2.23 (t, *J* = 6.9 Hz, 2H), 1.66–1.56 (m, 2H), 1.47 (s, 9H), 1.27–1.18 (m, 22H). <sup>13</sup>C NMR (100 MHz, CDCl<sub>3</sub>) δ 173.83, 169.58, 82.69, 63.94, 55.35, 36.51, 31.57, 29.63, 29.60, 29.56, 29.43, 29.29, 29.26, 29.21, 27.93, 25.54.

(*S*)-*N*-*d*<sub>5</sub>-palmitoyl-*O*-*H*-phosphonate-serine *tert*-butyl ester (**3c**). The **3c** was prepared from **2c** (0.71 g, 1.75 mmol, 1 eq), imidazole (2 g, 29.75 mmol, 25 eq), phosphorus trichloride (0.76 ml, 8.75 mmol, 5 eq), and triethylamine (3.65 ml, 26.25 mmol, 15 eq) according to the procedure described for the preparation of **3a**. The crude **3c** was used directly in the next step without purification.

(*S*)-*N*-*d*<sub>5</sub>-palmitoyl-*O*-phosphocholineserine *tert*-butyl ester (**5c**). The **5c** was prepared from crude **3c** (prepared as above), choline tetraphenylborate (1.48 g, 3.5 mmol, 2 eq), 2-chloro-5,5-dimethyl-1,3,2-dioxaphosphorinane 2-oxide (0.97 g, 5.25 mmol, 3 eq), iodine (0.533 g, 2.1, 1.2 eq), and water (0.4 ml) according to the procedure described for the preparation of **5a**. The crude **5c** was used directly in the next step without purification.

(*S*)-*N*-*d*<sub>5</sub>-palmitoyl-*O*-phosphocholineserine. The (*S*)-*N*-*d*<sub>5</sub>-palmitoyl-*O*-phosphocholineserine (*d*<sub>5</sub>-PPCS) was prepared as a white solid from crude **5c** (prepared as above), trifluoroacetic acid (20 ml), and chloroform (20 ml) according to the procedure described for the preparation of PPCS (85 mg, 9% overall yield from **2c**), mp: 221–223°C. <sup>1</sup>H NMR (400 MHz, CD<sub>3</sub>OD) δ 4.87 (s, 1H), 4.36 (d, 1H, *J* = 1.1 Hz), 4.22 (m, 2H), 4.07 (m, 1H), 3.58 (dd, 2H, *J* = 4.3, 6.2 Hz), 3.26 (d, 1H, *J* = 1.1 Hz), 3.17 (s, 9H), 2.22 (t, 2H, *J* = 7.6 Hz), 1.57 (m, 2H), 1.23 (m, 22H). <sup>13</sup>C NMR (100 MHz, CD<sub>3</sub>OD) δ 175.98, 174.78, 67.50, 67.44, 60.65, 60.60, 55.88, 55.80, 54.87, 54.83, 54.80, 37.26, 32.95, 30.98, 30.96, 30.83, 30.71, 30.61, 27.05.

Synthesis of *N*-*d*<sub>5</sub>-palmitoylserine (**6**), *N*-*d*<sub>5</sub>-palmitoylphosphatidylserine [*N*-*d*<sub>5</sub>-palmitoyl 1,2-distearoyl-*sn*-glycero-3-phospho-*L*-serine (**7**)], *N*-*d*<sub>5</sub>-palmitoyl-phytosphingosine phosphocholine (**8**), *N*-*d*<sub>5</sub>-palmitoyl-phosphoserine (**9**), and *O*-phosphocholine-*d*<sub>5</sub>-*L*-serine (**10**) is described in the supplemental information.

## Generation of PPCS in heathy human blood and quantification of PPCS in tissues from NPC animal models

The generation of PPCS in heathy human blood and quantification of PPCS in tissues from NPC animal models are described in the supplemental information.

## Profiling of APCS in human plasma

Profiling of APCS in human plasma is described in the supplemental information.

## Statistical methods

Normally distributed data were analyzed using Student's *t*-test or ANOVA. Non-normally distributed data was analyzed using the Mann-Whitney test or the Kruskal-Wallis test.

## RESULTS

### Elucidation of the structure of lysoSM-509

To elucidate the structure of lysoSM-509, we collected the HPLC fractions containing lysoSM-509 from NPC1 plasma and submitted the material for mass spectrometric

analysis and chemical derivatization. As it was difficult to isolate sufficient (at least 10  $\mu\text{g}$ ) pure endogenous lysoSM-509 from limited NPC plasma samples for acceptable NMR spectra due to its low abundance and the complex plasma lipid components, NMR analysis was not performed. Our strategy for determination of the structure of lysoSM-509 is outlined in Fig. 1.

**MS.** High-resolution mass spectrometric analysis of lysoSM-509 in the positive mode showed an abundant ion at an accurate  $m/z$  value of 509.3351 for  $[\text{M}+\text{H}]^+$  corresponding to the formula  $\text{C}_{24}\text{H}_{50}\text{O}_7\text{N}_2\text{P}$  (calculated mass, 509.3350) with mass errors less than 1 mDa (Fig. 2A). The  $[\text{M}+\text{Na}]^+$  ion at  $m/z$  531.3168 ( $\text{C}_{24}\text{H}_{49}\text{O}_7\text{N}_2\text{PNa}$ ; calculated mass, 531.3170) and the  $[\text{M}+2\text{Na}-\text{H}]^+$  ion at  $m/z$  553.2986 ( $\text{C}_{24}\text{H}_{48}\text{O}_7\text{N}_2\text{PNa}_2$ ; calculated mass, 553.2989) were also observed in positive mode (Fig. 2A), and the  $[\text{M}-\text{H}]^-$  ion at  $m/z$  507.3205 ( $\text{C}_{24}\text{H}_{48}\text{O}_7\text{N}_2\text{P}$ ; calculated mass, 507.3205) appeared in negative mode (Fig. 2B), suggesting that there were two acidic groups in lysoSM-509. The molecular formula  $\text{C}_{24}\text{H}_{50}\text{O}_7\text{N}_2\text{P}$  indicated that the degree of unsaturation in lysoSM-509 was two.

The high-resolution and accurate-mass product ion spectrum (Fig. 2C) of the  $[\text{M}+\text{H}]^+$  ion acquired with higher energy collisional dissociation (HCD) contained product ions at  $m/z$  184.0730, 124.9997, 104.1072, and 86.0968, corresponding to protonated phosphocholine ( $\text{C}_5\text{H}_{15}\text{NO}_4\text{P}^+$ ; calculated mass, 184.0733), protonated ethylene phosphate ( $\text{C}_2\text{H}_6\text{O}_4\text{P}^+$ ; calculated mass, 124.9998), choline ( $\text{C}_5\text{H}_{14}\text{NO}^+$ ; calculated mass, 104.1070), vinyltrimethylammonium ( $\text{C}_5\text{H}_{12}\text{N}^+$ ; calculated mass, 86.0964), respectively, indicating that lysoSM-509 contains a phosphocholine group (33). Very low abundant product ions at  $m/z$  326.2697 ( $\text{C}_{19}\text{H}_{36}\text{NO}_3^+$ ; calculated mass, 326.2690; resulted from neutral loss of a phosphocholine),  $m/z$  271.1045 ( $\text{C}_8\text{H}_{20}\text{N}_2\text{O}_6\text{P}^+$ ; calculated mass, 271.1053), and  $m/z$  225.0996 ( $\text{C}_7\text{H}_{18}\text{N}_2\text{OP}^+$ ; calculated mass, 225.0999) were also observed. Fragmentation of the  $[\text{M}+\text{Na}]^+$  and  $[\text{M}+2\text{Na}-\text{H}]^+$  ions provided information only related to phosphocholine. The product ions of the  $[\text{M}+\text{Na}]^+$  ion include  $m/z$  472.2430 ( $[\text{M}+\text{Na}-\text{N}(\text{CH}_3)_3]^+$ ,  $\text{C}_{21}\text{H}_{40}\text{NO}_7\text{PNa}$ ; calculated mass, 472.2435),  $m/z$  348.2511 ( $[\text{M}+\text{Na}-\text{phosphocholine}]^+$ ,

$\text{C}_{19}\text{H}_{35}\text{NO}_3\text{Na}^+$ ; calculated mass, 348.2509),  $m/z$  206.0552 ( $[\text{phosphocholine}+\text{Na}]^+$ ,  $\text{C}_5\text{H}_{14}\text{NO}_4\text{PNa}^+$ ; calculated mass, 206.0553),  $m/z$  146.9819 ( $[\text{ethylene phosphate}+\text{Na}]^+$ ,  $\text{C}_2\text{H}_5\text{O}_4\text{PNa}^+$ ; calculated mass, 146.9818), and  $m/z$  86.0964 (vinyltrimethylammonium,  $\text{C}_5\text{H}_{12}\text{N}^+$ ; calculated mass, 86.0964) (Fig. 2D). HCD of the  $[\text{M}+2\text{Na}-\text{H}]^+$  ion gave  $m/z$  494.2258 ( $[\text{M}+\text{Na}_2-\text{H}-\text{N}(\text{CH}_3)_3]^+$ ,  $\text{C}_{21}\text{H}_{39}\text{NO}_7\text{PNa}_2^+$ ; calculated mass, 494.2254),  $m/z$  370.2325 ( $[\text{M}+2\text{Na}-\text{H}-\text{phosphocholine}]^+$ ,  $\text{C}_{19}\text{H}_{34}\text{NO}_3\text{Na}_2^+$ ; calculated mass, 370.2329),  $m/z$  228.0370 ( $[\text{phosphocholine}+2\text{Na}-\text{H}]^+$ ,  $\text{C}_5\text{H}_{13}\text{NO}_4\text{PNa}_2^+$ ; calculated mass, 228.0372),  $m/z$  206.0553 ( $[\text{phosphocholine}+\text{Na}]^+$ ,  $\text{C}_5\text{H}_{14}\text{NO}_4\text{PNa}^+$ ; calculated mass, 206.0553),  $m/z$  168.9638 ( $[\text{ethylene phosphate}-\text{H}+2\text{Na}]^+$ ,  $\text{C}_2\text{H}_4\text{O}_4\text{PNa}_2^+$ ; calculated mass, 168.9637), and  $m/z$  86.0964 (vinyltrimethylammonium,  $\text{C}_5\text{H}_{12}\text{N}^+$ ; calculated mass, 86.0964) (Fig. 2E). The HCD spectrum of the  $[\text{M}-\text{H}]^-$  ion shows product ions at  $m/z$  324.2551 ( $[\text{M}-\text{H}-\text{phosphocholine}]^-$ ,  $\text{C}_{19}\text{H}_{34}\text{NO}_3^-$ ; calculated mass, 324.2544),  $m/z$  280.2653 ( $\text{C}_{18}\text{H}_{34}\text{NO}^-$ ; calculated mass, 280.2646),  $m/z$  237.2228 ( $\text{C}_{16}\text{H}_{29}\text{O}^-$ ; calculated mass, 237.2224),  $m/z$  168.0435 ( $[\text{phosphocholine}-\text{CH}_3]^-$ ,  $\text{C}_4\text{H}_{11}\text{NO}_4\text{P}^-$ ; calculated mass, 168.0435),  $m/z$  122.9856 ( $[\text{ethylene phosphate}-\text{H}]^-$ ,  $\text{C}_2\text{H}_4\text{O}_4\text{P}^-$ ; calculated mass, 122.9856),  $m/z$  96.9699 ( $\text{H}_2\text{PO}_4^-$ ; calculated mass, 96.9699), and  $m/z$  78.9592 ( $\text{PO}_3^-$ ; calculated mass, 78.9591) (Fig. 2F). Although product ions at  $m/z$  271.1045 and 225.0996 from fragmentation of protonated lysoSM-509 and  $m/z$  280.2653 and 237.2228 ions from fragmentation of deprotonated lysoSM-509 provided structural information for other than phosphocholine, the structure of lysoSM-509 could not be assigned without more information.

Although the full mass scan of lysoSM-509 offered a good quality spectrum, the H/D exchange experiment using the full mass scan did not provide sufficient sensitivity as the signals were distributed over additional isotope peaks, and the amount of HPLC-isolated lysoSM-509 was limited. MRM was used to detect the deuterium exchange-associated peaks, in which MRM transitions from deuterium exchanged lysoSM-509 to protonated phosphocholine were used. A number of possible deuterated precursors included  $[\text{M}+\text{H}]^+$  at  $m/z$  509,  $[\text{M}+\text{D}]^+$  at  $m/z$  510,  $[\text{M}-\text{H}+2\text{D}]^+$  at  $m/z$  511,  $[\text{M}-2\text{H}+3\text{D}]^+$  at  $m/z$  512,  $[\text{M}-3\text{H}+4\text{D}]^+$  at  $m/z$

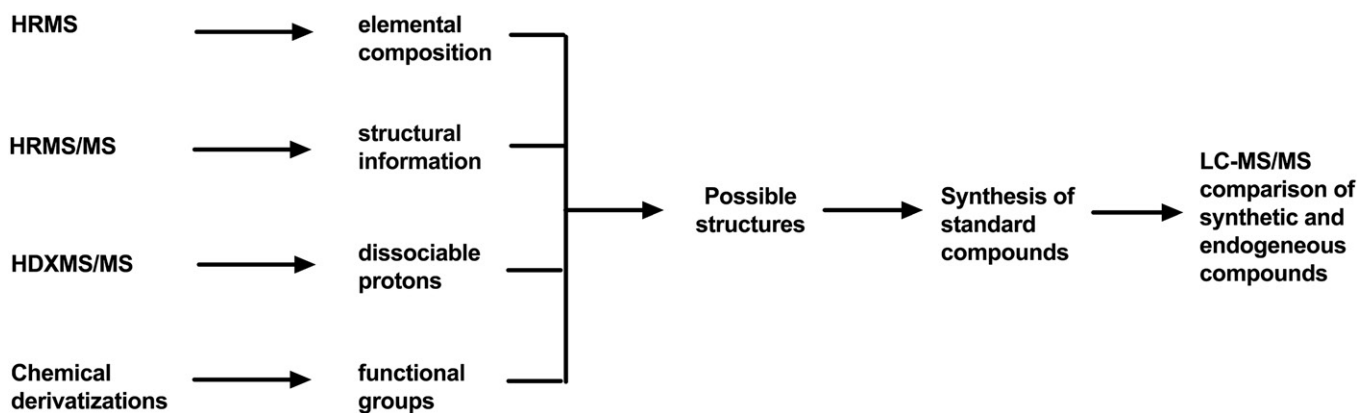


**Fig. 1.** Strategy for identification of lysoSM-509 structure. HRMS, high-resolution MS; HRMS/MS, high-resolution MS/MS; HDXMS/MS, H/D exchange MS/MS.

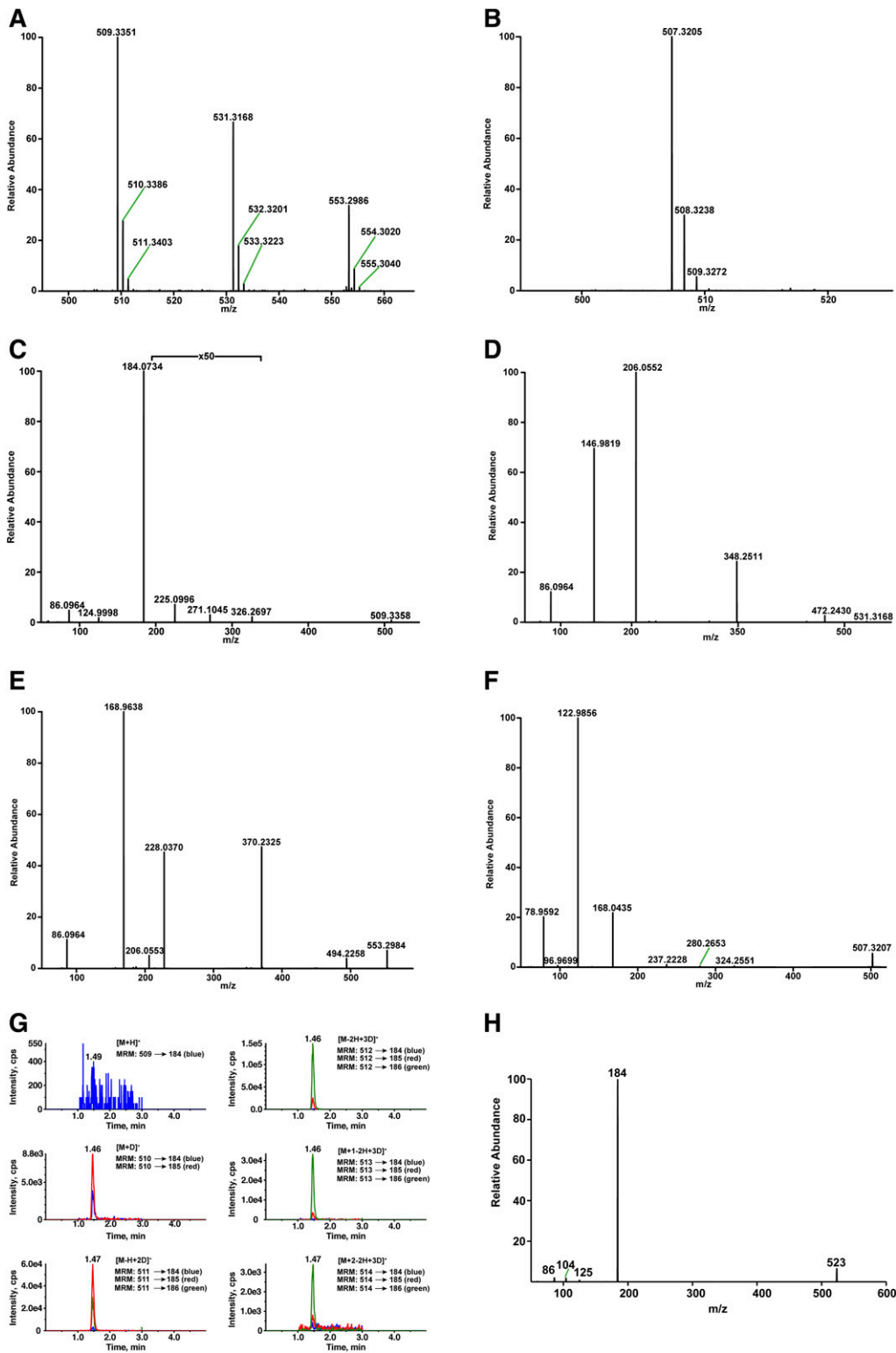


**Fig. 2.** Identification of the structure of lysoSM-509. A: High-resolution mass spectrum of endogenous lysoSM-509 in positive ion mode. B: High-resolution mass spectrum of endogenous lysoSM-509 in negative ion mode. C: High-resolution product ion spectrum of the  $[M+H]^+$  ion of endogenous lysoSM-509. D: High-resolution product ion spectrum of the  $[M+Na]^+$  ion of endogenous lysoSM-509. E: High-resolution product ion spectrum of the  $[M+2Na-H]^+$  ion of endogenous lysoSM-509. F: High-resolution product ion spectrum of the  $[M-H]^-$  ion of endogenous lysoSM-509. G: H/D exchange of endogenous lysoSM-509 detected with MRM. The  $[M+2H+3D]^+$  ion at  $m/z$  512 shows the maximum intensity. H: Product ion spectrum of the  $[M+H]^+$  ion of endogenous lysoSM-509 methyl ester.

513, and  $[M-4H+5D]^+$  at  $m/z$  514. Protonated phosphocholine was used to construct the MRM transitions. There are two labile hydrogens in protonated phosphocholine, and deuterated phosphocholine was also included (supplemental Table S1). The number of exchangeable hydrogens is the difference between the mass of the exchanged peak with maximum intensity and the mass of the  $[M+D]^+$  at  $m/z$  510. The  $[M-2H+3D]^+$  at  $m/z$  512 showed the maximum intensity, showing that there were two exchangeable protons in lysoSM-509 (Fig. 2G).

**Chemical derivatization.** Treatment of lysoSM-509 with HCl in methanol gave a methyl ester with mass upshift of 14 Da (Fig. 2H), suggesting that lysoSM-509 bore a carboxylic group. The fragmentation of the  $[M+H]^+$  ion of the methyl ester produced the same product ions as those in lysoSM-509. The toleration of acidic conditions by lysoSM-509 indicated that there were no acid-labile groups, such as a vinyl ether or an imine. No acetylated products were observed when lysoSM-509 was treated with acetic anhydride/pyridine, suggesting that it did not have nucleophiles such as amino and alcohol groups. lysoSM-509 survived the treatment with ozone, suggesting that it lacked a carbon-carbon double bond. Treatment of lysoSM-509 with sodium hydroxide in methanol-water (95:5) led to decomposition. Two decomposition products (decomposition product 1, *N*-palmitoylserine; decomposition product 2, *N*-palmitoyl-*O*-methylserine) were confirmed only after authentic PPCS was synthesized.

**Proposed structure of lysoSM-509.** We proposed that the phosphocholine was connected to the other moiety of lysoSM-509 via a phosphate bond, similar to phosphatidylcholine and sphingomyelin, because protonated phosphocholine is also the most abundant product ion in fragmentation of  $[M+H]^+$  of phosphatidylcholine and sphingomyelin. Besides the phosphocholine and carboxylic groups, the remaining moiety of lysoSM-509 had a formula of  $C_{18}H_{35}ON$ , in which the oxygen and nitrogen were most likely part of an amide bond. The presence of the carboxylic acid and the amide groups in lysoSM-509 was in agreement with the degree of unsaturation of two, no amine or alcohol group, and two exchangeable protons. After assignment of phosphocholine, carboxylic acid, and the amide groups, the remaining  $C_{17}H_{34}$  was composed of saturated alkyl groups. lysoSM-509 was temporarily assigned as PPCS.

The structure of PPCS was supported by the proposed fragmentation pathways to all the product ions from the  $[M+H]^+$  ion (Fig. 3A). The  $m/z$  326 ion was formed by intramolecular attack of the carboxylate to the phosphocholine, resulting in loss of a phosphocholine. Loss of palmitoyl as a ketene gave the  $m/z$  271 ion. The 1,4-elimination led to loss of a  $CO_2$  and a palmitaldehyde to yield the  $m/z$  225 ion. The dominant product ion at  $m/z$  184 was generated via six-membered ring H-transfer as a major pathway and 1,2-elimination as a minor pathway, which were supported by the H/D exchange experiment. The  $m/z$  184 ion also was generated from the  $m/z$  271 ion after loss of a  $CO_2$  and

a vinylamine via 1,4-elimination. Further neutral loss of trimethylamine, metaphosphoric acid, and phosphoric acid from the  $m/z$  184 ion yielded the  $m/z$  125, 104, and 86 ions, respectively.

Unlike other phosphocholine lipids, such as phosphatidylcholine and sphingomyelin, that produce the  $[M-15]^-$  ion by neutral loss of  $CH_3X$  via collisional decomposition of the adduct anion  $[M+X]^-$  at the orifice, where X can be chloride, formate, and acetate (34), PPCS readily formed the  $[M-H]^-$  ion due to the carboxylic acid group. The structure of PPCS was also supported by fragmentation of the  $[M-H]^-$  ion. The 1,2-elimination of a phosphocholine afforded the  $m/z$  324 ion. The 1,4-elimination led to loss of a  $CO_2$  and a phosphocholine to yield the  $m/z$  280 ion, which underwent 1,4-elimination of a vinylamine to give the  $m/z$  237 ion. Formation of the  $m/z$  168 ion was probably via attack of methyl on choline by the carboxylate followed by 1,2-elimination to yield demanyl phosphate at  $m/z$  168, from which neutral loss of *N*-vinyl dimethylamine and 2-dimethylaminoethanol gave phosphate ( $m/z$  97) and metaphosphate ( $m/z$  79), respectively. The  $m/z$  123 ion was generated after neutral loss of the lactone and trimethylamine from the  $[M-H]^-$  ion (Fig. 3B).

### Synthesis of PPCS

In order to confirm the structure of PPCS, we devised a synthetic plan to generate PPCS. Accordingly, we prepared *N*-palmitoyl-L-serine methyl ester (2a) and converted it to *N*-palmitoyl-*O*-phosphocholineserine methyl ester (5a) via H-phosphonate intermediates 3a and 4a using a modified literature procedure (35) (Fig. 4A). The nonhygroscopic choline tetraphenylborate (36) was used for installation of the H-phosphocholine in 4a. However, base hydrolysis of the methyl ester in 5a led to two decomposition products, *N*-palmitoylserine (decomposition product 1) and *N*-palmitoyl-*O*-methylserine (decomposition product 2), in which the phosphocholine group was lost. Although base hydrolysis of a typical sphingomyelin cleaves the phosphoester bond on the choline side to yield ceramide-1-phosphate (37), the phosphoester bond at the serine side of PPCS was cleaved. This unusual cleavage may be due to the intramolecular participation of the carboxylate group, which attacks carbon-3 of serine to give a four-membered ring lactone. The lactone was unstable due to ring strain and readily opened by attack of hydroxide and methoxide to afford decomposition products 1 and 2 (Fig. 4B). This issue was addressed in a revised approach, in which the methyl ester-protecting group was changed to a *tert*-butyl ester. Following the same procedure as for 5a, *N*-palmitoyl-*O*-phosphocholineserine *tert*-butyl ester (5b) was prepared. Removal of the *tert*-butyl ester in 5b with trifluoroacetic acid afforded PPCS. The crude synthetic intermediates, 3a/b to 5a/b, were used directly in the next step without isolation, which significantly simplified the synthetic procedure. PPCS was purified with reverse phase solid phase extraction followed by chromatography on silica. Similarly,  $d_5$ -PPCS was also prepared as an internal standard for quantification of PPCS from *N*- $d_5$ -palmitoyl-L-serine *tert*-butyl ester (2c).

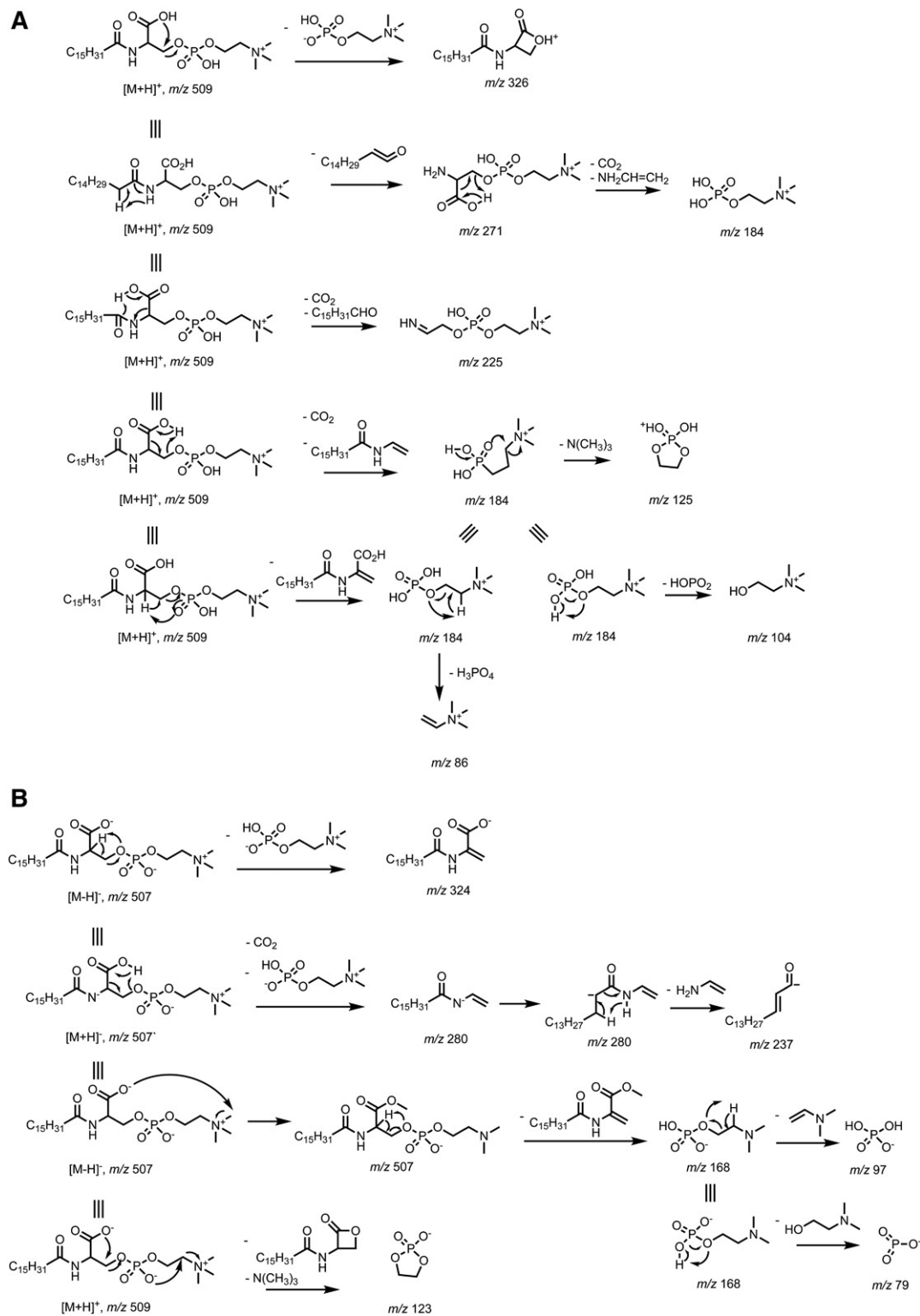


**Fig. 3.** Proposed fragmentation pathways for PPCS. A: Proposed fragmentation pathway for the  $[M+H]^+$  ion. B: Proposed fragmentation pathway for the  $[M-H]^-$  ion.

### Confirmation of the structure of lysoSM-509

The structure of lysoSM-509 was confirmed by comparative LC-MS/MS analysis of endogenous and synthesized authentic compound, its methyl esters, and decomposition products under basic conditions. Endogenous lysoSM-509

(**Fig. 5A, B**) and its methyl ester (**Fig. 5C**) showed the same retention time and product ion scan spectra as synthetic PPCS and its methyl ester, respectively. The decomposition products of endogenous lysoSM-509 were detected with MRM of all the abundant product ions from

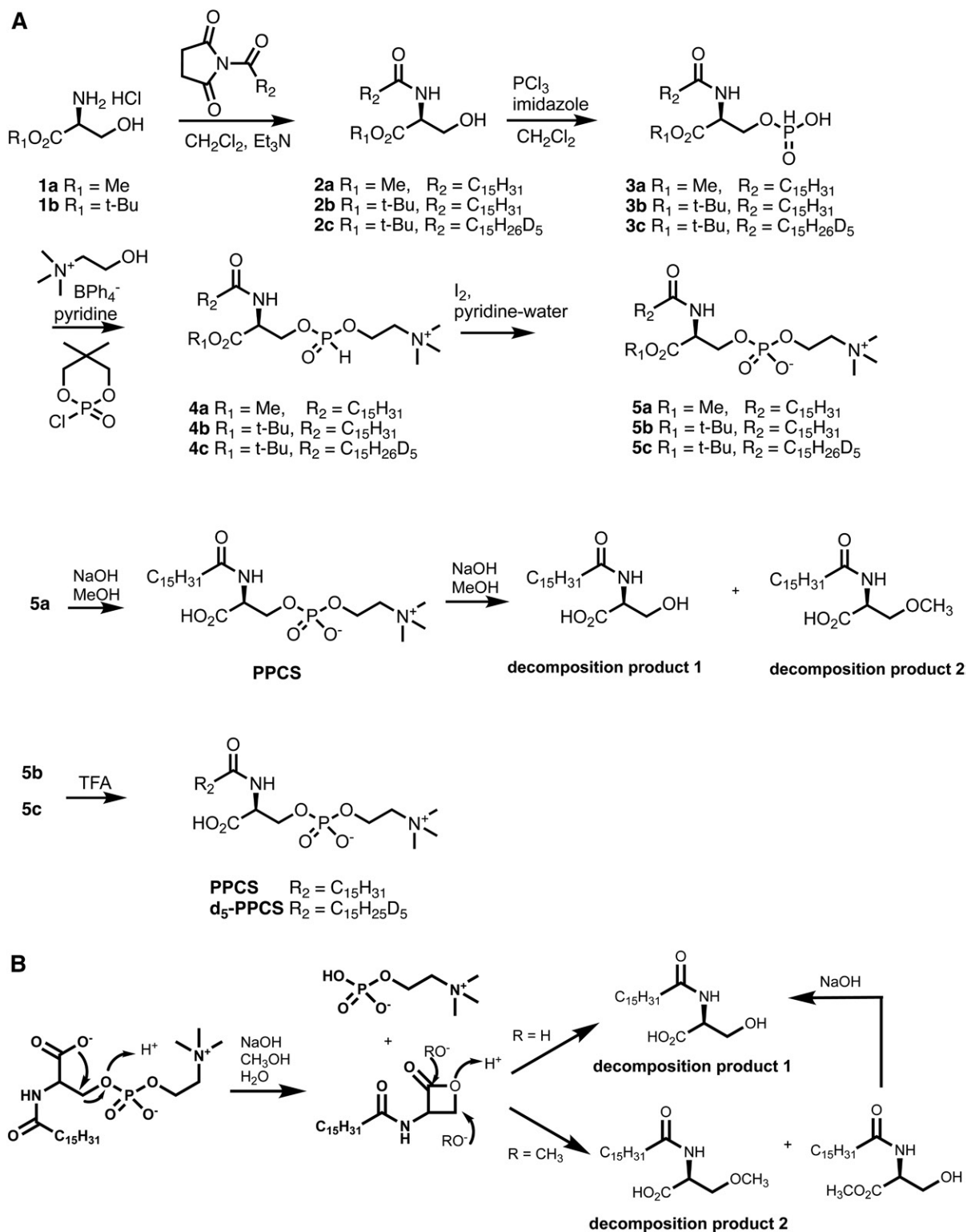


**Fig. 4.** Synthesis of PPCS and d<sub>5</sub>-PPCS (A) and proposed mechanism for the formation of decomposition products 1 and 2 (B).

collision-induced dissociation of the decomposition products of synthetic PPCS (supplemental Fig. S1), because they were not sufficiently abundant to provide good quality product ion spectra. The decomposition products of endogenous lysoSM-509 matched with those of synthetic PPCS (**Fig. 5D**). All of the results verified that lysoSM-509 is PPCS.

#### Generation of PPCS in human blood

To explore the ability of PPCS to serve as a biomarker for newborn screening of NPC1 disease, we compared newborn controls (n = 211), NPC1 carriers (n = 10), and NPC1 subjects (n = 10). Compared with newborn controls, PPCS in dried blood spots from NPC1 subjects was elevated only 2.75-fold with overlap between two groups (**Fig. 6A**), whereas



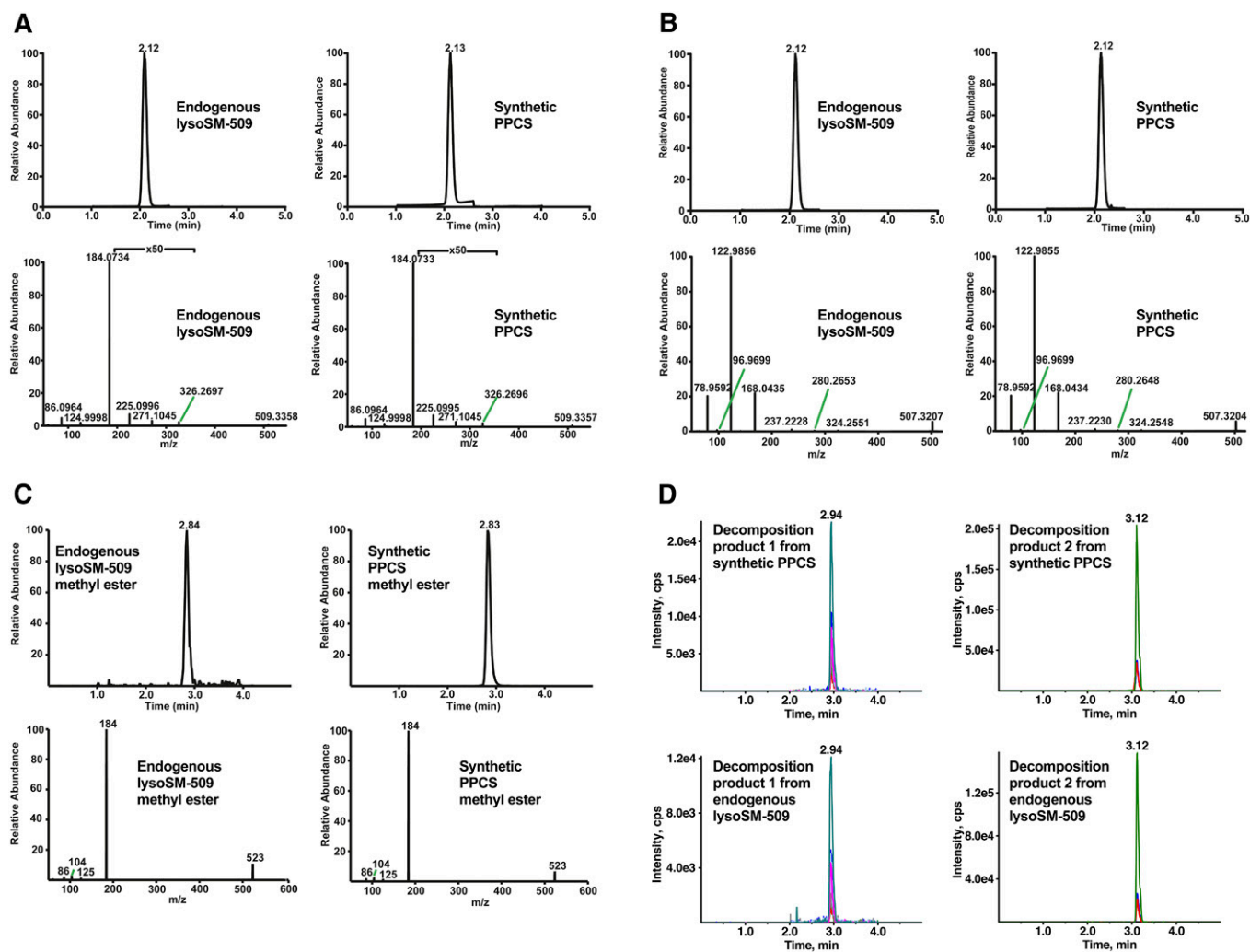


**Fig. 5.** Confirmation of the structure of lysoSM-509. A: Chromatograms (detected by product ion scan) and high resolution product ion spectra of the  $[M+H]^+$  ions of endogenous lysoSM-509 and synthetic PPCS. B: Chromatograms (detected by product ion scan) and high-resolution product ion spectra of the  $[M-H]^-$  ions of endogenous lysoSM-509 and synthetic PPCS. C: Chromatograms (detected by product ion scan) and product ion spectra of the  $[M+H]^+$  ions of endogenous lysoSM-509 methyl ester and synthetic PPCS methyl ester. D: Decomposition products 1 and 2 from synthetic PPCS and endogenous lysoSM-509. Decomposition product 1 was detected in seven MRM transitions. Decomposition product 2 was detected in three MRM transitions.

PPCS was elevated 24-fold in NPC1 plasma compared with control plasma (Fig. 6B). The overlap between PPCS in NPC1 and control dried blood spots has also been reported in an earlier report (28).

PPCS in blank Whatman 903 newborn screening cards was undetectable. To investigate the basis of attenuated PPCS in dried blood spots compared with plasma, we examined PPCS in whole blood and dried blood spots from the same normal subjects. Compared with whole blood, PPCS in dried blood spots increased 8.3-fold (Fig. 6C). To determine whether components in the Whatman 903 newborn screening card promoted PPCS production in whole blood, we agitated whole blood with 3 mm disks from a blank newborn screening card for 18 h at room temperature. The PPCS levels in blood with newborn screening card disks did not change (not shown), suggesting that PPCS was generated during the drying process. We further compared the PPCS in red blood cells, white blood cells, and plasma with dried red blood cell spots,

dried white blood cell spots, and dried plasma spots, respectively. Although PPCS was not detectable in red blood cells and white blood cells, PPCS levels in dried red blood cell spots and white blood cell spots ranged from 60 to 83 ng/ml red blood cells and from 62 to 72 ng/dried white blood cells from 3 ml whole blood, respectively (Fig. 6D, E). Similarly, PPCS in dried plasma spots increased 4-fold compared with plasma levels (Fig. 6F). These results indicate that a PPCS precursor is present in all the blood components and can be converted into PPCS during drying.

We spiked several potential precursors to explore the biosynthetic route of the PPCS, including  $N$ - $d_5$ -palmitoyl-serine (6),  $N$ - $d_5$ -palmitoylphosphatidylserine [ $N$ - $d_5$ -palmitoyl 1,2-distearoyl-*sn*-glycero-3-phospho-L-serine (7)],  $N$ - $d_5$ -palmitoyl-phytosphingosine phosphocholine (8),  $N$ - $d_5$ -palmitoyl-phosphoserine (9),  $O$ -phosphocholine- $d_3$ -L-serine (10), and  $d_5$ -palmitic acid (11) into blood and prepared dried blood spots. However, neither  $d_5$ -PPCS nor  $d_3$ -PPCS was observed in the dried blood spots, indicating that

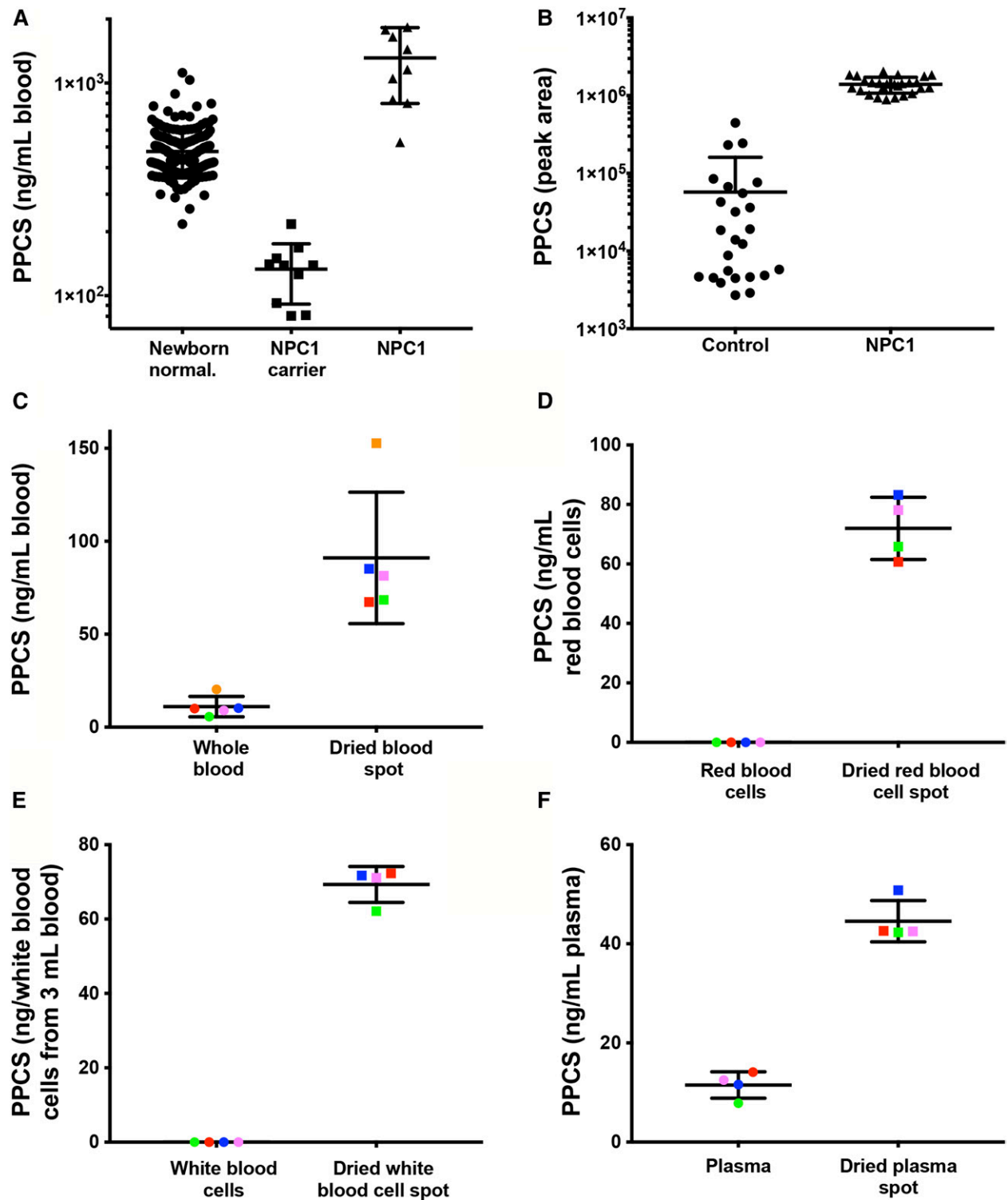


**Fig. 6.** PPCS in dried blood spot and plasma samples and its generation in blood during the drying process. **A:** PPCS in newborn control ( $n = 211$ ), NPC1 carrier ( $n = 10$ ), and NPC1 ( $n = 10$ ) dried blood spot samples. Data are presented as mean  $\pm$  95% confidence interval (CI) concentration.  $P < 0.0001$  for lysoSM-509 in NPC1 versus controls and NPC1 carriers. **B:** PPCS in control ( $n = 25$ ) and NPC1 ( $n = 26$ ) plasma samples. Data are presented as mean  $\pm$  95% CI peak area.  $P < 0.0001$  for lysoSM-509 in NPC1 versus controls. **C:** Elevation of PPCS in dried blood spots ( $n = 5$ ) compared with whole blood ( $n = 5$ ). The dried blood spots and whole blood from the same subject are shown in the same color. Data are presented as mean  $\pm$  95% CI.  $P < 0.0001$  for dried blood spots versus whole blood. **D:** Elevation of PPCS in dried red blood cell spots ( $n = 4$ ) compared with red blood cells ( $n = 4$ ). The dried red blood cell spots and red blood cells from the same subject are shown in the same color. Data are presented as mean  $\pm$  95% CI.  $P < 0.0001$  for dried red blood cell spots versus red blood cells. **E:** Elevation of PPCS in dried white blood cell spots ( $n = 4$ ) compared with white blood cells ( $n = 4$ ). The dried white blood cell spots and white blood cells from the same subject are shown in the same color. Data are presented as mean  $\pm$  95% CI.  $P < 0.0001$  for dried white blood cell spots versus white blood cells. **F:** Elevation of PPCS in dried plasma spots ( $n = 4$ ) compared with plasma ( $n = 4$ ). The dried plasma spots and plasma from the same subject are shown in the same color. Data are presented as mean  $\pm$  95% CI.  $P < 0.0001$  for dried plasma spots versus plasma.

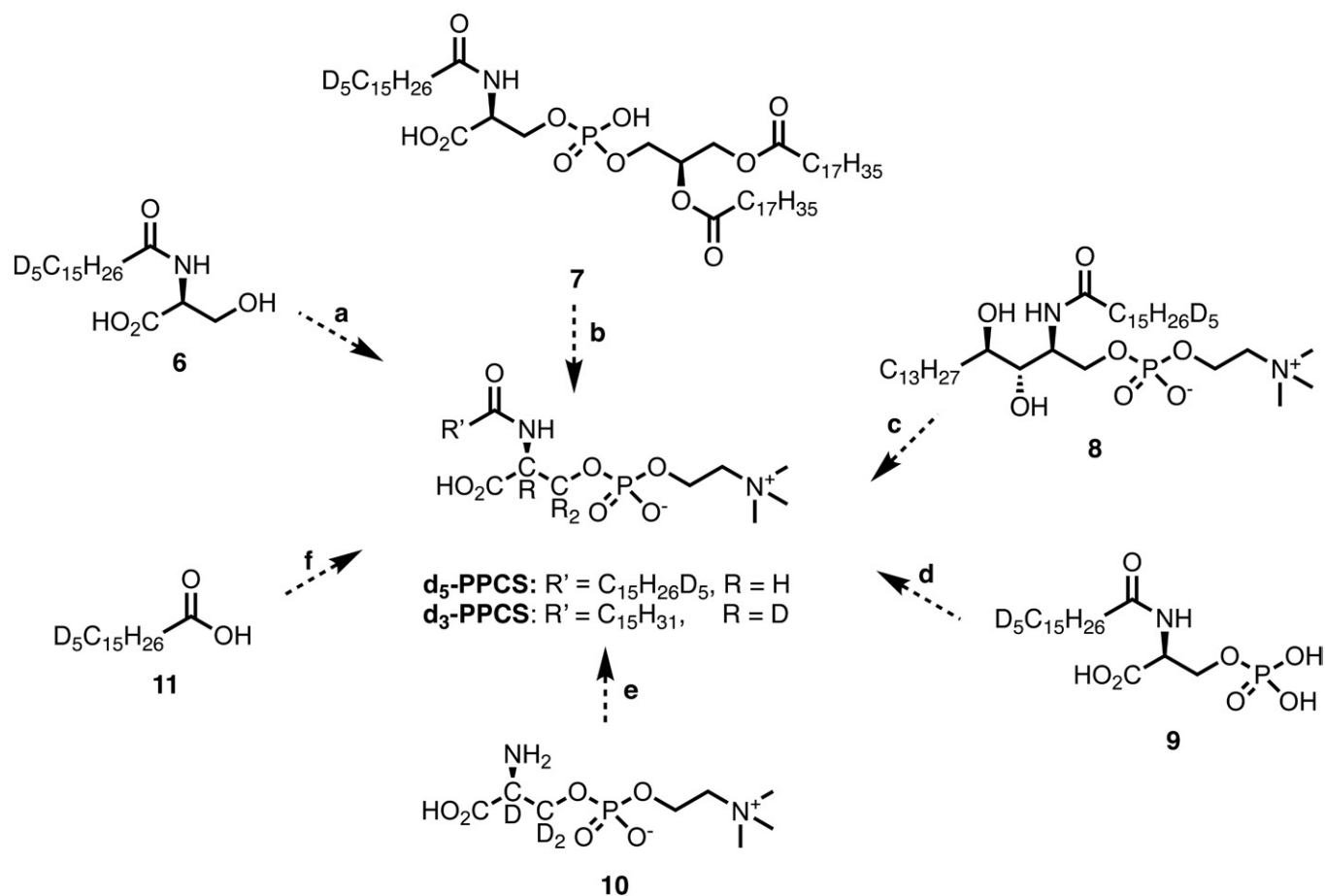


**Fig. 7.** Hypothetical pathways for the formation of PPCS. Neither  $d_5$ -PPCS nor  $d_3$ -PPCS were formed in dried blood spots from potential precursors, including  $N$ - $d_5$ -palmitoylserine (6),  $N$ - $d_5$ -palmitoylphosphatidylserine ( $N$ - $d_5$ -palmitoyl 1,2-distearoyl-*sn*-glycero-3-phospho-L-serine) (7),  $N$ - $d_5$ -palmitoyl-phytosphingosine phosphocholine (8),  $N$ - $d_5$ -palmitoyl-phosphoserine (9),  $O$ -phosphocholine- $d_3$ -L-serine (10), and  $d_5$ -palmitic acid (11).

none of these compounds appeared to be direct precursors of PPCS (Fig. 7).

#### Elevation of PPCS in serum, brain, and liver from a NPC1 cat model

To understand whether PPCS is elevated in the central nervous system or peripheral organs in NPC1 disease, we analyzed plasma/serum, brain, and liver from NPC1 mouse and cat models. While PPCS was undetectable in plasma and tissues from mouse (data not shown), it was significantly elevated in serum, brain, and liver in NPC1 cats compared with control and NPC1 carrier cats (Fig. 8). This result demonstrated that PPCS accumulates in both central and peripheral tissues and highlighted the species difference between mouse and cat/human with respect to metabolic pathways involved in generation of PPCS.

#### APCS in human plasma

The structure of PPCS [APCS(16:0)] suggested that it was one of multiple species in the APCS lipid family. We also analyzed other species in plasma using MRM transitions from theoretical masses of  $[M+H]^+$  ions of APCS to  $m/z$  184 (Table 1). The APCS species included  $N$ -myristoyl- [APCS(14:0)],  $N$ -palmitoyl- [APCS(16:0)],

$N$ -palmitoleoyl- [APCS(16:1)],  $N$ -stearoyl- [APCS(18:0)],  $N$ -oleoyl- [APCS(18:1)],  $N$ -arachidoyl- [APCS(20:0)],  $N$ -behenoyl- [APCS(22:0)],  $N$ -lignoceroyl- [APCS(24:0)], and tetracosenoyl- $O$ -phosphocholineserines [APCS(24:1)]. Like PPCS, all other APCS species were elevated in NPC1 plasma (Fig. 9).

## DISCUSSION

Diagnosis of NPC1 disease is challenging due to the rare nature of the disorder, the genetic heterogeneity, and the initially nonspecific clinical presentation. The advent of NPC1 disease-specific biochemical markers has shortened the time to diagnosis of patients with a high clinical suspicion of NPC1, in which the disease is significantly advanced. Nonetheless, biomarkers that can be applied to the general population or for newborn screening could further improve early identification of the disease. One such marker, lysoSM-509, is currently under evaluation as a NPC1 diagnostic marker (27), and LC-MS/MS diagnostic assays based on lysoSM-509 have been reported (28–31). However, quantification of lysoSM-509 using these assays has not been reliable due to lack of information regarding the

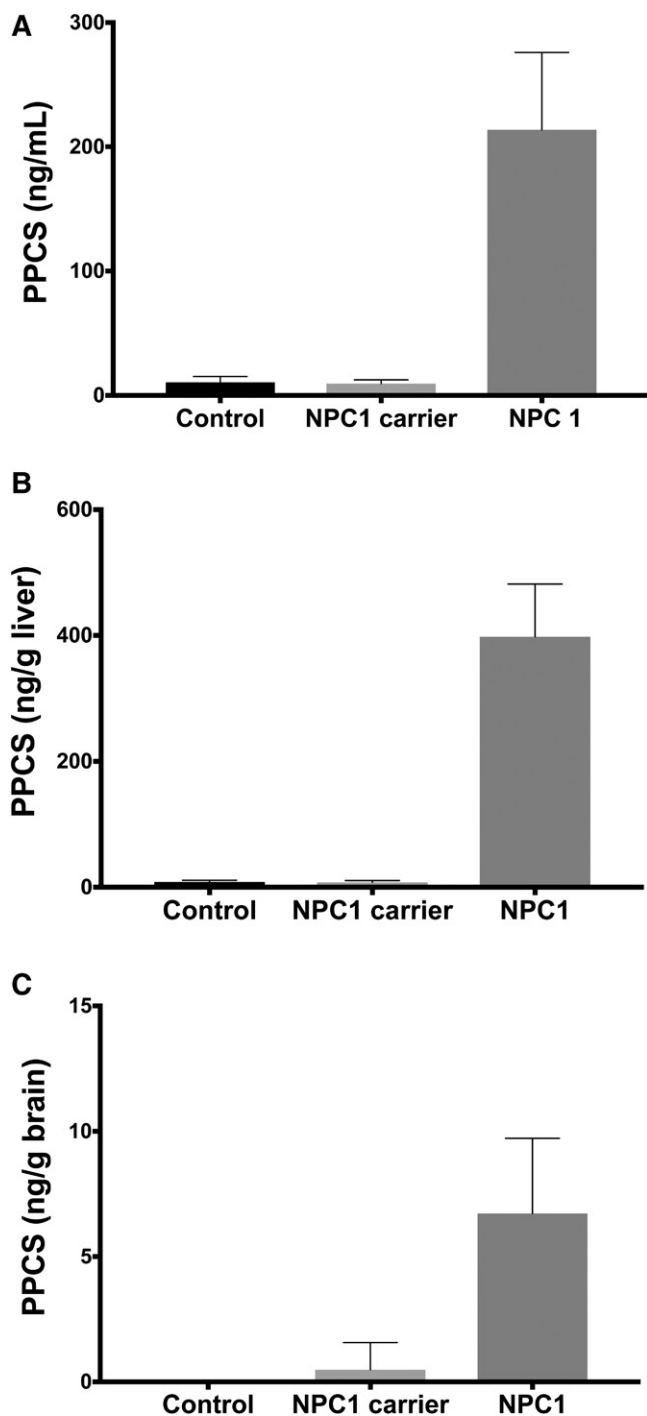


**Fig. 8.** Elevation of PPCS in serum, brain, and liver from NPC1 cat model. **A:** PPCS in sera from control ( $n = 8$ ), NPC1 carrier ( $n = 3$ ), and NPC1 ( $n = 7$ ) cats. Data are presented as mean with SD.  $P < 0.0001$  for NPC1 versus control and NPC carriers. **B:** PPCS in livers from control ( $n = 9$ ), NPC1 carrier ( $n = 5$ ), and NPC1 ( $n = 5$ ) cats. Data are presented as mean with SD.  $P < 0.0001$  for NPC1 versus control and NPC carriers. **C:** PPCS in brains from control ( $n = 10$ ), NPC1 carrier ( $n = 5$ ), and NPC1 ( $n = 6$ ) cats. Data are presented as mean with SD.  $P < 0.0001$  for NPC1 versus control and NPC carriers.

molecular identity of the biomarker. As no authentic standard was available, lysosphingomyelin was used as a calibrator. The mass spectrometric responses of lysoSM-509 and lysosphingomyelin and their matrix effects are different,

TABLE 1. MRM transitions for APCS

MRM Transition	APCS	Precursor Ion ( $m/z$ )	Product Ion ( $m/z$ )
1	APCS(14:0)	481.3	184
2	APCS(16:0)	509.3	184
3	APCS(16:1)	507.3	184
4	APCS(18:0)	537.3	184
5	APCS(18:1)	535.3	184
6	APCS(20:0)	565.3	184
7	APCS(22:0)	593.3	184
8	APCS(24:0)	621.3	184
9	APCS(24:1)	619.3	184


and it is always best to use a chemically identical but isotopically substituted lysoSM-509 internal standard. In the present study, we identified the structure of lysoSM-509 by accurate mass measurements, tandem mass spectra, chemical derivatization, and comparison to an authentic synthetic standard. Unexpectedly, we found that lysoSM-509 is not a lysosphingomyelin species, as previously proposed (27). Rather, the biomarker is PPCS, a member of a unique class of lipids designated as APCS. With the structure of lysoSM-509 in hand, it is now possible to synthesize and use a proper internal standard for its accurate quantification.

To the best of our knowledge, APCS lipids have not previously been described. A series of related serine compounds have been reported in biological samples, including *O*-serine phosphoethanolamine (38), *N*-acylserines (39), *N*-acyl lysophosphatidylserines (40), and *N*-acyl phosphatidylserines (39, 41). Serine phosphoethanolamine was identified with  $^{31}\text{P}$ NMR in dystrophic chicken (38). *N*-acyl phosphatidylserines were originally identified in sheep red blood cells by infrared spectrum, elemental analysis, and hydrolysis products (41). Later, *N*-acyl phosphatidylserines and *N*-acylserines were identified in human brain with the palmitoyl and stearoyl forms being most abundant when analyzed by MS, and their levels change in the frontal cortex in schizophrenia (39). *N*-acyl phosphatidylserines were also detected with LC-MS/MS in pig brain, mouse RAW264.7 macrophage tumor cells, and yeast (42). *N*-arachidonoyl serine is an activator of large conductance  $\text{Ca}^{2+}$ -activated  $\text{K}^{+}$  channels (43) with vasodilatory properties (44), which also alters the activation of N-type  $\text{Ca}^{2+}$  channels in sympathetic neurons (45). *N*-acyl lysophosphatidylserines were identified in mouse brain with mass spectrometric lipidomics, and ABHD4 is a general *N*-acyl phospholipid hydrolase to convert *N*-acyl phosphatidylserines to *N*-acyl lysophosphatidylserines (40). *N*-palmitoylserine phosphoric acid was synthesized as inhibitor of lipid phosphatidate receptors (46). *O*-phosphocholine-L-serine has not been reported previously, and we synthesized *O*-phosphocholine- $\text{d}_3$ -L-serine (10) as a potential precursor to study biosynthesis of PPCS in this study.

Although we observed artifactual generation of PPCS in blood components from normal subjects, including whole blood, red blood cells, white blood cells, and plasma, when they were dried on newborn screening cards, PPCS is an endogenous lipid that is stable in blood and plasma under normal experimental conditions. The PPCS level in whole blood did not change at room temperature after the blood was agitated with 3 mm disks from a blank newborn

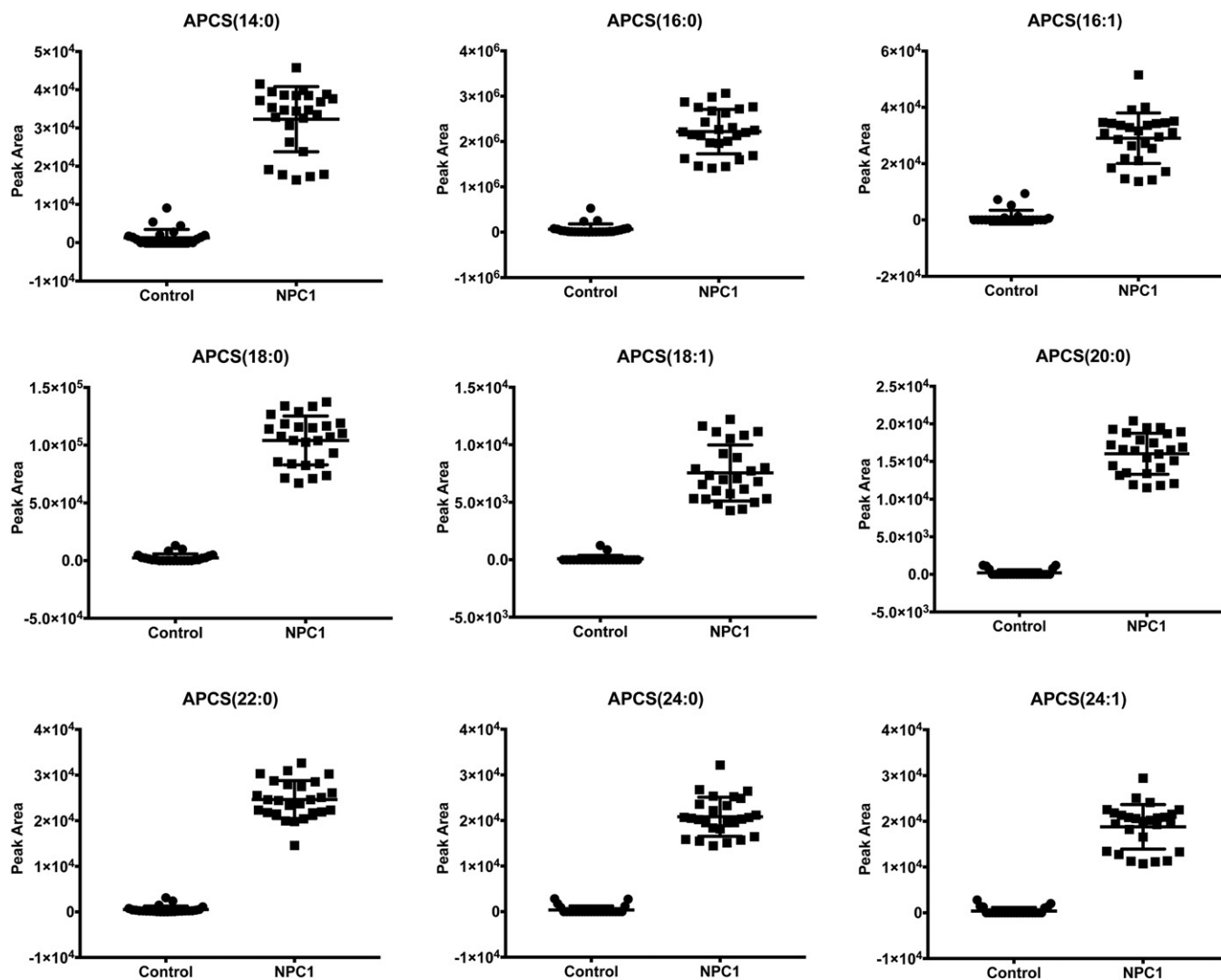


**Fig. 9.** APCS in human plasma. APCS including *N*-myristoyl- [APCS(14:0)], *N*-palmitoyl- [APCS(16:0)], *N*-palmitoleoyl- [APCS(16:1)], *N*-stearoyl- [APCS(18:0)], *N*-oleoyl- [APCS(18:1)], *N*-arachidoyl- [APCS(20:0)], *N*-behenoyl- [APCS(22:0)], *N*-lignoceroyl [APCS(24:0)], and tetracosenoyl-*O*-phosphocholineserines [APCS(24:1)] in control ( $n = 25$ ) and NPC1 ( $n = 26$ ) plasma samples. Data are presented as mean  $\pm$  95% CI peak area.  $P < 0.0001$  for all APCS species in NPC1 versus controls.

screening card for 18 h. We also developed a validated plasma assay for PPCS that will be published in a separate article, and found that the PPCS level in plasma was unchanged at room temperature for 24 h. Artfactual generation of PPCS in blood on newborn screening cards significantly reduced the difference in PPCS levels between NPC1 and normal subjects. As a result, we observed significant overlap between NPC1 and newborn controls, consistent with an earlier report (28), thus rendering PPCS of limited utility for NPC newborn screening based on detection of the metabolite in dried blood spots. Although our effort to elucidate the biosynthesis of APCS using blood drying on newborn screening cards in this study was not successful, our work has eliminated a number of possibilities and provided a foundation for future study. Understanding the biosynthesis and regulation of APCS and its involvement in NPC and acid sphingomyelinase deficiency, in which plasma PPCS levels are increased (27), may uncover the potential therapeutic targets for these two storage diseases. 

The authors would like to thank Dr. Douglas Covey for helpful discussion of the synthesis of PPCS. The authors are grateful to the National Niemann-Pick Disease Foundation for their assistance in obtaining samples from NPC1 and NPC1 carrier subjects and express their appreciation to the families and patients who participated in this study.

## REFERENCES

1. Carstea, E. D., J. A. Morris, K. G. Coleman, S. K. Loftus, D. Zhang, C. Cummings, J. Gu, M. A. Rosenfeld, W. J. Pavan, D. B. Krizman, et al. 1997. Niemann-Pick C1 disease gene: homology to mediators of cholesterol homeostasis. *Science*. **277**: 228–231.
2. Naureckiene, S., D. E. Sleat, H. Lackland, A. Fensom, M. T. Vanier, R. Wattiaux, M. Jadot, and P. Lobel. 2000. Identification of HE1 as the second gene of Niemann-Pick C disease. *Science*. **290**: 2298–2301.
3. Vanier, M. T. 2010. Niemann-Pick disease type C. *Orphanet J. Rare Dis.* **5**: 16.
4. Walkley, S. U., and K. Suzuki. 2004. Consequences of NPC1 and NPC2 loss of function in mammalian neurons. *Biochim. Biophys. Acta*. **1685**: 48–62.
5. Bonnot, O., C. S. Gama, E. Mengel, M. Pineda, M. T. Vanier, L. Watson, M. Watissee, B. Schwierin, and M. C. Patterson. 2019.

- Psychiatric and neurological symptoms in patients with Niemann-Pick disease type C (NP-C): Findings from the International NPC Registry. *World J. Biol. Psychiatry*. **20**: 310–319.
6. Vanier, M. T., P. Gissen, P. Bauer, M. J. Coll, A. Burlina, C. J. Hendriks, P. Latour, C. Goizet, R. W. Welford, T. Marquardt, et al. 2016. Diagnostic tests for Niemann-Pick disease type C (NP-C): A critical review. *Mol. Genet. Metab*. **118**: 244–254.
  7. Fecarotta, S., A. Romano, R. Della Casa, E. Del Giudice, D. Bruschini, G. Mansi, B. Bembì, A. Dardis, A. Fiumara, M. Di Rocco, et al. 2015. Long term follow-up to evaluate the efficacy of miglustat treatment in Italian patients with Niemann-Pick disease type C. *Orphanet J. Rare Dis*. **10**: 22.
  8. Ory, D. S., E. A. Ottinger, N. Y. Farhat, K. A. King, X. Jiang, L. Weissfeld, E. Berry-Kravis, C. D. Davidson, S. Bianconi, L. A. Keener, et al. 2017. Intrathecal 2-hydroxypropyl-beta-cyclodextrin decreases neurological disease progression in Niemann-Pick disease, type C1: a non-randomised, open-label, phase 1–2 trial. *Lancet*. **390**: 1758–1768.
  9. Berry-Kravis, E., J. Chin, A. Hoffmann, A. Winston, R. Stoner, L. LaGorio, K. Friedmann, M. Hernandez, D. S. Ory, F. D. Porter, et al. 2018. Long-term treatment of Niemann-Pick type C1 disease with intrathecal 2-hydroxypropyl-beta-cyclodextrin. *Pediatr. Neurol*. **80**: 24–34.
  10. Maarup, T. J., A. H. Chen, F. D. Porter, N. Y. Farhat, D. S. Ory, R. Sidhu, X. Jiang, and P. I. Dickson. 2015. Intrathecal 2-hydroxypropyl-beta-cyclodextrin in a single patient with Niemann-Pick C1. *Mol. Genet. Metab*. **116**: 75–79.
  11. Jiang, X., R. Sidhu, F. D. Porter, N. M. Yanjanin, A. O. Speak, D. T. te Vruchte, F. M. Platt, H. Fujiwara, D. E. Scherrer, J. Zhang, et al. 2011. A sensitive and specific LC-MS/MS method for rapid diagnosis of Niemann-Pick C1 disease from human plasma. *J. Lipid Res*. **52**: 1435–1445.
  12. Porter, F. D., D. E. Scherrer, M. H. Lanier, S. J. Langmade, V. Molugu, S. E. Gale, D. Olzeski, R. Sidhu, D. J. Dietzen, R. Fu, et al. 2010. Cholesterol oxidation products are sensitive and specific blood-based biomarkers for Niemann-Pick C1 disease. *Sci. Transl. Med*. **2**: 56ra81.
  13. Boenzi, S., F. Deodato, R. Taurisano, D. Martinelli, D. Verrigni, R. Carozzo, E. Bertini, A. Pastore, C. Dionisi-Vici, and D. W. Johnson. 2014. A new simple and rapid LC-ESI-MS/MS method for quantification of plasma oxysterols as dimethylaminobutyrate esters. Its successful use for the diagnosis of Niemann-Pick type C disease. *Clin. Chim. Acta*. **437**: 93–100.
  14. Klinke, G., M. Rohrbach, R. Giugliani, P. Burda, M. R. Baumgartner, C. Tran, M. Gautschi, D. Mathis, and M. Hersberger. 2015. LC-MS/MS based assay and reference intervals in children and adolescents for oxysterols elevated in Niemann-Pick diseases. *Clin. Biochem*. **48**: 596–602.
  15. Pajares, S., A. Arias, J. Garcia-Villoria, J. Macias-Vidal, E. Ros, J. de las Heras, M. Giros, M. J. Coll, and A. Ribes. 2015. Cholestane-3beta,5alpha,6beta-triol: high levels in Niemann-Pick type C, cerebrotendinous xanthomatosis, and lysosomal acid lipase deficiency. *J. Lipid Res*. **56**: 1926–1935.
  16. Kannenberg, F., J. R. Nofer, E. Schulte, J. Reunert, T. Marquardt, and M. Fobker. 2017. Determination of serum cholestane-3beta,5alpha,6beta-triol by gas chromatography-mass spectrometry for identification of Niemann-Pick type C (NPC) disease. *J. Steroid Biochem. Mol. Biol*. **169**: 54–60.
  17. Reunert, J., M. Fobker, F. Kannenberg, I. Du Chesne, M. Plate, J. Wellhausen, S. Rust, and T. Marquardt. 2015. Rapid diagnosis of 83 patients with Niemann Pick type C disease and related cholesterol transport disorders by cholestantriol screening. *EBioMedicine*. **4**: 170–175.
  18. Romanello, M., S. Zampieri, N. Bortolotti, L. Deroma, A. Sechi, A. Fiumara, R. Parini, B. Borroni, F. Brancati, A. Bruni, et al. 2016. Comprehensive evaluation of plasma 7-ketocholesterol and cholestan-3beta,5alpha,6beta-triol in an Italian cohort of patients affected by Niemann-Pick disease due to NPC1 and SMPD1 mutations. *Clin. Chim. Acta*. **455**: 39–45.
  19. Bauer, P., D. J. Balding, H. H. Klunemann, D. E. Linden, D. S. Ory, M. Pineda, J. Priller, F. Sedel, A. Muller, H. Chadha-Boreham, et al. 2013. Genetic screening for Niemann-Pick disease type C in adults with neurological and psychiatric symptoms: findings from the ZOOM study. *Hum. Mol. Genet*. **22**: 4349–4356.
  20. Reunert, J., A. S. Lotz-Havla, G. Polo, F. Kannenberg, M. Fobker, M. Griese, E. Mengel, A. C. Muntau, P. Schnabel, O. Sommerburg, et al. 2015. Niemann-Pick type C-2 disease: identification by analysis of plasma cholestane-3beta,5alpha,6beta-triol and further insight into the clinical phenotype. *JIMD Rep*. **23**: 17–26.
  21. Zhang, H., Y. Wang, N. Lin, R. Yang, W. Qiu, L. Han, J. Ye, and X. Gu. 2014. Diagnosis of Niemann-Pick disease type C with 7-ketocholesterol screening followed by NPC1/NPC2 gene mutation confirmation in Chinese patients. *Orphanet J. Rare Dis*. **9**: 82.
  22. Hammerschmidt, T. G., G. de Oliveira Schmitt Ribas, M. L. Saraiva-Pereira, M. P. Bonatto, R. G. Kessler, F. T. S. Souza, F. Trapp, K. Michelin-Tirelli, M. G. Burin, R. Giugliani, et al. 2018. Molecular and biochemical biomarkers for diagnosis and therapy monitoring of Niemann-Pick type C patients. *Int. J. Dev. Neurosci*. **66**: 18–23.
  23. Polo, G., A. Burlina, F. Furlan, T. Kolamunnage, M. Cananzi, L. Giordano, M. Zaninotto, M. Plebani, and A. Burlina. 2016. High level of oxysterols in neonatal cholestasis: a pitfall in analysis of biochemical markers for Niemann-Pick type C disease. *Clin. Chem. Lab. Med*. **54**: 1221–1229.
  24. Welford, R. W., M. Garzotti, C. Marques Lourenco, E. Mengel, T. Marquardt, J. Reunert, Y. Amraoui, S. A. Kolb, O. Morand, and P. Groenen. 2014. Plasma lysosphingomyelin demonstrates great potential as a diagnostic biomarker for Niemann-Pick disease type C in a retrospective study. *PLoS One*. **9**: e114669.
  25. Jiang, X., R. Sidhu, L. Mydock-McGrane, F. F. Hsu, D. F. Covey, D. E. Scherrer, B. Earley, S. E. Gale, N. Y. Farhat, F. D. Porter, et al. 2016. Development of a bile acid-based newborn screen for Niemann-Pick disease type C. *Sci. Transl. Med*. **8**: 337ra63.
  26. Mazzacuva, F., P. Mills, K. Mills, S. Camuziaux, P. Gissen, E. R. Nicoli, C. Wassif, D. Te Vruchte, F. D. Porter, M. Maekawa, et al. 2016. Identification of novel bile acids as biomarkers for the early diagnosis of Niemann-Pick C disease. *FEBS Lett*. **590**: 1651–1662.
  27. Giese, A. K., H. Mascher, U. Grittner, S. Eichler, G. Kramp, J. Lukas, D. te Vruchte, N. Al Eisa, M. Cortina-Borja, F. D. Porter, et al. 2015. A novel, highly sensitive and specific biomarker for Niemann-Pick type C1 disease. *Orphanet J. Rare Dis*. **10**: 78.
  28. Kuchar, L., J. Sikora, M. E. Gulinello, H. Poupetova, A. Lugowska, V. Malinova, H. Jahnova, B. Asfaw, and J. Ledvinova. 2017. Quantitation of plasmatic lysosphingomyelin and lysosphingomyelin-509 for differential screening of Niemann-Pick A/B and C diseases. *Anal. Biochem*. **525**: 73–77.
  29. Pettazzoni, M., R. Froissart, C. Pagan, M. T. Vanier, S. Ruet, P. Latour, N. Guffon, A. Fouilhoux, D. P. Germain, T. Levade, et al. 2017. LC-MS/MS multiplex analysis of lysosphingolipids in plasma and amniotic fluid: A novel tool for the screening of sphingolipidoses and Niemann-Pick type C disease. *PLoS One*. **12**: e0181700.
  30. Polo, G., A. P. Burlina, T. B. Kolamunnage, M. Zampieri, C. Dionisi-Vici, P. Strisciuglio, M. Zaninotto, M. Plebani, and A. B. Burlina. 2017. Diagnosis of sphingolipidoses: a new simultaneous measurement of lysosphingolipids by LC-MS/MS. *Clin. Chem. Lab. Med*. **55**: 403–414.
  31. Voorink-Moret, M., S. M. I. Goorden, A. B. P. van Kuilenburg, F. A. Wijburg, J. M. M. Ghauharali-van der Vlugt, F. S. Beers-Stet, A. Zoetekouw, W. Kulik, C. E. M. Hollak, and F. M. Vaz. 2018. Rapid screening for lipid storage disorders using biochemical markers. Expert center data and review of the literature. *Mol. Genet. Metab*. **123**: 76–84.
  32. Patterson, M. C., P. Clayton, P. Gissen, M. Anheim, P. Bauer, O. Bonnot, A. Dardis, C. Dionisi-Vici, H. H. Klunemann, P. Latour, et al. 2017. Recommendations for the detection and diagnosis of Niemann-Pick disease type C: An update. *Neurol. Clin. Pract*. **7**: 499–511.
  33. Hsu, F. F., and J. Turk. 2003. Electrospray ionization/tandem quadrupole mass spectrometric studies on phosphatidylcholines: the fragmentation processes. *J. Am. Soc. Mass Spectrom*. **14**: 352–363.
  34. Murphy, R. C., and P. H. Axelsen. 2011. Mass spectrometric analysis of long-chain lipids. *Mass Spectrom. Rev*. **30**: 579–599.
  35. Lindh, I., and J. Stawifski. 1989. A general method for the synthesis of glycerophospholipids and their analogues via H-phosphonate intermediates. *J. Org. Chem*. **54**: 1338–1342.
  36. Harbison, G. S., and R. G. Griffin. 1984. Improved method for the synthesis of phosphatidylcholines. *J. Lipid Res*. **25**: 1140–1142.
  37. Wijesinghe, D. S., J. C. Allegood, L. B. Gentile, T. E. Fox, M. Kester, and C. E. Chalfant. 2010. Use of high performance liquid chromatography-electrospray ionization-tandem mass spectrometry for the analysis of ceramide-1-phosphate levels. *J. Lipid Res*. **51**: 641–651.
  38. Chalovich, J. M., C. T. Burt, S. M. Cohen, T. Glonek, and M. Barany. 1977. Identification of an unknown 31P nuclear magnetic resonance from dystrophic chicken as L-serine ethanolamine phosphodiester. *Arch. Biochem. Biophys*. **182**: 683–689.

39. Wood, P. L. 2014. Accumulation of N-acylphosphatidylserines and N-acylserines in the frontal cortex in schizophrenia. *Neurotransmitter (Houst.)*. **1**: e263.
40. Lee, H. C., G. M. Simon, and B. F. Cravatt. 2015. ABHD4 regulates multiple classes of N-acyl phospholipids in the mammalian central nervous system. *Biochemistry*. **54**: 2539–2549.
41. Nelson, G. J. 1970. Studies on the lipids of sheep red blood cells. IV. The identification of a new phospholipid. N-acyl phosphatidyl serine. *Biochem. Biophys. Res. Commun.* **38**: 261–265.
42. Guan, Z., S. Li, D. C. Smith, W. A. Shaw, and C. R. Raetz. 2007. Identification of N-acylphosphatidylserine molecules in eukaryotic cells. *Biochemistry*. **46**: 14500–14513.
43. Godlewski, G., L. Offertaler, D. Osei-Hyiaman, F. M. Mo, J. Harvey-White, J. Liu, M. I. Davis, L. Zhang, R. K. Razdan, G. Milman, et al. 2009. The endogenous brain constituent N-arachidonoyl L-serine is an activator of large conductance Ca<sup>2+</sup>-activated K<sup>+</sup> channels. *J. Pharmacol. Exp. Ther.* **328**: 351–361.
44. Milman, G., Y. Maor, S. Abu-Lafi, M. Horowitz, R. Gallily, S. Batkai, F. M. Mo, L. Offertaler, P. Pacher, G. Kunos, et al. 2006. N-arachidonoyl L-serine, an endocannabinoid-like brain constituent with vasodilatory properties. *Proc. Natl. Acad. Sci. USA*. **103**: 2428–2433.
45. Guo, J., D. J. Williams, and S. R. Ikeda. 2008. N-arachidonoyl L-serine, a putative endocannabinoid, alters the activation of N-type Ca<sup>2+</sup> channels in sympathetic neurons. *J. Neurophysiol.* **100**: 1147–1151.
46. Bittman, R., B. Swords, K. Liliom, and G. Tigy. 1996. Inhibitors of lipid phosphatidate receptors: N-palmitoyl-serine and N-palmitoyl-tyrosine phosphoric acids. *J. Lipid Res.* **37**: 391–398.